PHOTONICS Research

Graded index fiber as an all-fiber saturable absorber for large energy conventional soliton and dissipative soliton generation

ZHAOKUN WANG, JIKAI CHEN, TIANYU ZHU, D. N. WANG,* AND FENG GAO

College of Optical and Electronic Technology, China Jiliang University, Hangzhou 310018, China
*Corresponding author: dnwang@cjlu.edu.cn

Received 12 July 2019; revised 30 August 2019; accepted 31 August 2019; posted 4 September 2019 (Doc. ID 372621); published 10 October 2019

In this work, we investigate the possibility of achieving nanojoule level pulse energy in an all-fiber Er-doped oscillator by using a graded index multimode fiber (GIMF) as the saturable absorber (SA). This GIMF-based SA demonstrates the desirable characteristics of high-power tolerance, large modulation depth of 29.6%, and small saturation fluence of ~7.19 × 10^{-3} μJ/cm^2, which contribute to the high-energy soliton generation. In the experiments, the oscillator generates stable ultrafast pulse trains with high pulse energy/average output power up to 13.65 nJ/212.4 mW in the anomalous regime and 6.25 nJ/72.5mW in the normal regime, which are among the highest energy/average output power values achieved by all-fiber Er lasers. The results obtained demonstrate that the GIMF-based SA can be used as an effective photonic device for high-energy wave-breaking free pulse generation.

https://doi.org/10.1364/PRJ.7.001214

1. INTRODUCTION

The development of large-energy ultrafast fiber lasers in the telecom window (~1.5 μm) has attracted much interest due to their wide applications from terahertz-wave generation, frequency metrology to high-field physics, and so on [1–3]. However, the pulse energy is generally limited by the pulse-splitting phenomenon, which results from excessive nonlinearity accumulation [4]. Although an Er-doped fiber amplifier can be used to boost the pulse energy [5], it is subject to increased noise, system complexity, and associated cost. Dissipative soliton resonance (DSR) [6,7] without wave breaking allows the pulse energy to reach the 10 nJ level in mode-locked fiber lasers; however, the pulse width of DSR is usually broadened into hundreds of nanoseconds. A Mamyshev oscillator [8,9] is also an effective method for large energy soliton generation. Unfortunately, the oscillator with the free space configuration is bulky, which increases the complexity of the system. In past decades, it has been recognized that the extra spectral phase modulation added by the saturable absorber (SA) with a large modulation depth helps to suppress the pulse splitting [10–12]; hence, an ultrafast pulse with relatively high pulse energy can be achieved. Based on a $MoTe_2$ SA with a modulation depth of 22.1%, pulses with energy of 2.14 nJ in the 1.5 μm regime have been directly obtained [12]. An Er-doped fiber oscillator mode-locked by the atomic layer graphene provides 415 fs pulses of 7.3 nJ energy [13]. The use of a single-wall carbon nanotube SA (SWCNT-SA) [14] produces 594 fs and 7 nJ pulses with a repetition rate of 13.3 MHz. Inspired by the above-mentioned development of a large energy ultrafast fiber laser, researchers from different communities are trying their best to further develop new types of SAs.

Among them, SAs with all-fiber structures have the advantage of compactness and high efficiency and are less prone to damage than material SAs [15–19]. Recently, graded-index multimode fibers (GIMFs) have become an appealing platform for observing novel nonlinear optical phenomena [19–23], as they can play the role of an SA in mode-locked fiber lasers. Such an approach has been investigated theoretically [19] and demonstrated experimentally [23–27] since 2013. The GIMF-based SA has been reported to be used as SA in the Yb-doped [23,24], Er-doped [25,26], and Tm-doped [27,28] mode-locked fiber lasers and demonstrate the superior properties of controllable nonlinearity, simple structure, etc., in the near-infrared wavelength regime. Although the GIMF-based SA is an effective method for soliton generation, the achieved pulse energy is usually limited to a sub-nJ level. For the large energy operation, Chen *et al.* [25] obtained the conventional soliton (CS) energy of 0.38 nJ in an Er-doped fiber laser. However, these solitons cannot be maintained as stable and degenerate into stretched pulses with increased pump power. From this viewpoint, it is still a challenging task to generate high-energy soliton pulses by using such an all-fiber-structured SA.

In this paper, a GIMF-based SA with a large modulation depth of 29.6% and a small saturation fluence of ~7.19 × 10^{-3} μJ/cm^2 at 1.5 μm is proposed and demonstrated for high-energy pulse generation. By inserting a GIMF-based SA into an Er-doped fiber laser, 1.89 ps CSs with high pulse energy/average output power up to 13.65 nJ/212.4 mW in the

anomalous regime and 21.3 ps dissipative solitons (DSs) of 6.25 nJ/72.5 mW in the normal regime have been generated, respectively. To the best of our knowledge, the CSs have the highest output pulse energy and average power among the reported all-fiber Er-doped ultrafast pulse lasers. Such a mode-locked fiber laser shows many advantages such as simple structure, high slope efficiency, excellent environmental stability, which provides a simple way for construction of a large energy oscillator.

2. CHARACTERISTICS OF THE GIMF-BASED SA

Figure 1 shows a diagram of the SMF-GIMF-SMF structure. The GIMF-based SA device consists of a sandwiched GIMF section of length L, fusion spliced to the standard single-mode fibers (SMFs) (Corning SMF28e) at its ends. The length and the core/cladding size of the standard and commercially available GIMF used in our experiment are ~37 cm and 62.5/125 μm, respectively. The length of the GIMF used should be half-beat length (to allow generating a phase of $k\pi + \pi/2$, where $k = 0, 1, 2, \ldots$), which ensures that the maximum power is transferred from the fundamental mode to the other higher-order modes in the linear regime. The beat length of the GIMF is measured to be ~694 μm, which is consistent with the calculation result obtained from the formula $Z = \pi R/\sqrt{2\Delta}$, where Z is the beat length, R is the core radius of the GIMF, and Δ is the index step [29]. The saturable absorption mechanism benefits from the nonlinear multimode interference (NL-MMI) effect, especially the self-phase modulation (SPM) and cross-phase modulation (XPM) effects in the GIMF [14]. The SPM and XPM effects alter the refractive index of each mode and, consequently, reduce the energy transformation from fundamental mode to higher-order modes. Such a power-dependent transmission and intensity discrimination effect finally results in saturable absorption. Here, the GIMF with a mode area of up to ~50 times larger than that of the SMF can effectively reduce the incident pulse energy density onto the SA, which offers an attractive solution for scaling up the pulse energy and peak power in mode-locked fiber lasers and elevates the threshold of the SA device, when compared with the 2D material SA [12,13]. Moreover, the nearly instantaneous response of nonlinearities in GIMF is ideal for ultrashort pulse generation.

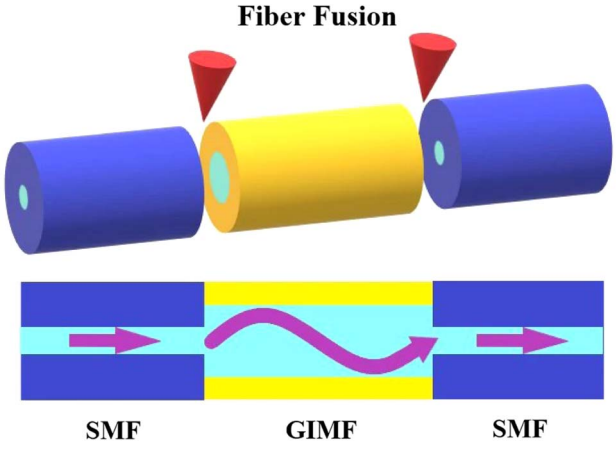

Fig. 1. Diagram of the GIMF-based saturable absorber.

For greater insight into the proposed SA device, which is suitable for large energy soliton generation, the nonlinear and linear characteristics need to be measured. Figure 2 illustrates a balanced twin-detector measurement system for measuring the nonlinear optical absorption properties of GIMF-based SA. The laser source is a homemade fiber laser, which is mode-locked by the nonlinear polarization rotation effect with a central wavelength of 1561 nm, pulse duration of 590 fs, and fundamental repetition frequency of 23.7 MHz. By using an optical attenuator, the average power could be deliberately controlled. The nonlinear saturable absorption curve is shown in Fig. 3. For simplification, the transmission curve is fitted as described by [30]

$$T(I) = 1 - \Delta T \times \exp\left(-\frac{I}{I_{\text{sat}}}\right) - \alpha_{\text{ns}}, \tag{1}$$

where T is the transmission, ΔT is the modulation depth, I is the input light intensity, I_{sat} is the saturation intensity, and α_{ns} is the nonsaturable loss. This method fits well with the experimental data. The absorption modulation depth is measured as 29.6%, and the value of saturation fluence is ~7.19×10^{-3} μJ/cm^2 (corresponding to the saturation intensity of ~1.21×10^{-2} MW/cm^2). Benefiting from the appropriate choice of the GIMF length, the energy mostly distributes in the higher-order modes at lower power, and a small coupling efficiency to the SMF is guaranteed. Thus, the GIMF-based SA demonstrates a relatively large modulation depth. The loss experienced by the high-intensity pulses with a large spectral bandwidth is much greater than that of the continuum wave (CW), as the CW can break up the pulse stability and limit the formation of the stable large energy solitons. Thus, the adoption of an SA with large modulation depth can provide more absorption to CW than to high-intensity pulses in the laser cavity, which compensates the spectral filtering loss and enhances the pulse energy. It should be highlighted that the saturation intensity is several orders of magnitude smaller than that of the 2D material. We speculate it may originate from the high Ge concentration and large length of the GIMF. Generally, the GIMF has a gradually rising dopant concentration (e.g., GeO_2) toward the fiber center, which provides a larger refractive-index than that of

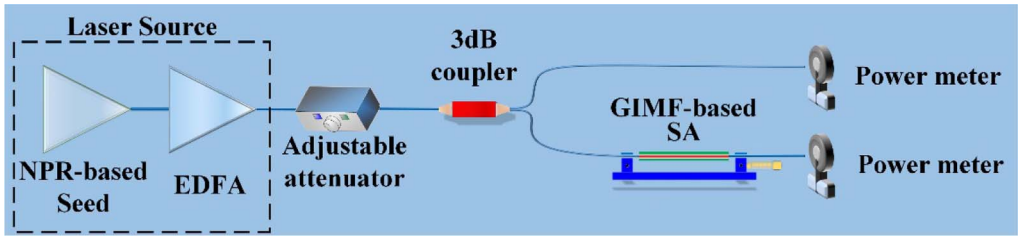

Fig. 2. Saturable absorption properties of stretched-GIMF SAs measured by the twin-detector measurement technique.

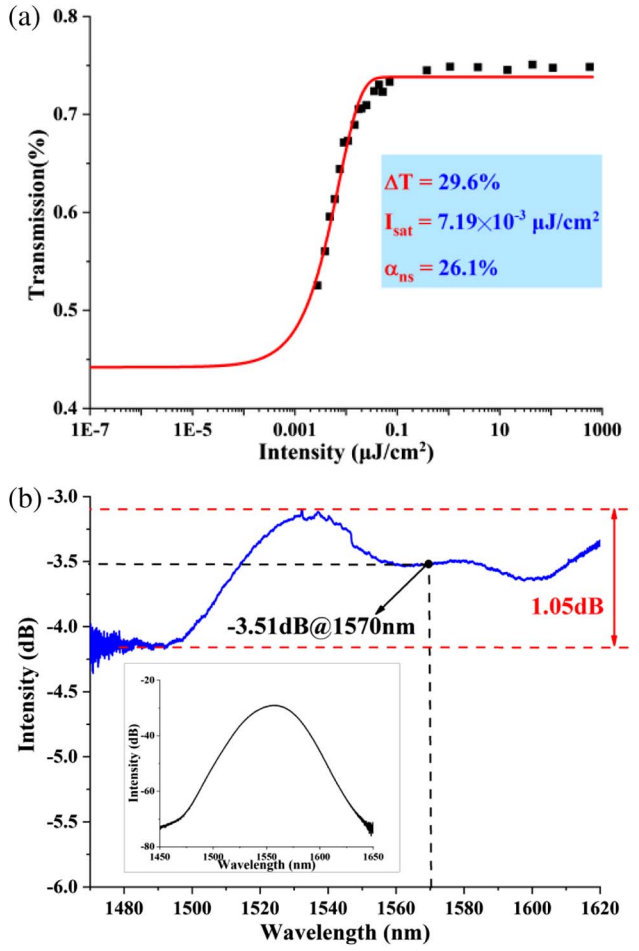

Fig. 3. (a) Nonlinear absorption curve and (b) linear transmission of the GIMF-SA device. Inset: Original spectrum of the broadband source.

the SMF. The relatively large refractive-index can raise the nonlinear coefficient and hence nonlinear strength of the GIMF. The length of GIMF is chosen to be hundreds of times larger than the beating length (~hundreds of micrometers) in GIMF, and the larger interaction length can contribute to a higher level of nonlinear effect and provide strong modulation of light. The increased nonlinear effect caused by the high Ge concentration and large length of the GIMF helps in lowering the saturation intensity [31]. With such a low saturable intensity, it can be predicted that the mode-locking operation can be easily realized, even though most of the pulse energy is extracted from the cavity. By taking advantage of saturable absorption property mentioned above, the GIMF-based SA can be developed into an effective passive nonlinear optical device for large energy pulse generation.

The linear transmission spectrum of the prepared GIMF-based SA is measured by using a supercontinuum broadband light source (BBS, Amonics) in the range from 1470 to 1620 nm. It is obtained by subtracting the transmission curve of the GIMF-based device from the spectral curve of the broadband source. As shown in Fig. 3(b), it has a relatively flat curve with the fluctuation of less than 1.1 dB; in other words, the transmission is not critically dependent on the operation wavelength. It can also be clearly seen from the figure that the signal transmission at the wavelength of 1570 nm is around 44.5%, which is consistent with the transmittance at the lower pulse intensity in Fig. 3(a).

3. MODE-LOCKED FIBER LASER FOR LARGE ENERGY SOLITONS

A. Schematic of the Large Energy Fiber Oscillator

A diagram of the experimental setup is shown in Fig. 4. It is a ring cavity consisting of a 70 cm long Er-doped fiber (EDF, Nufern SM-ESF-7/125) with an absorption of 50 dB @ 1530 nm, an optical coupler (OC), a polarization

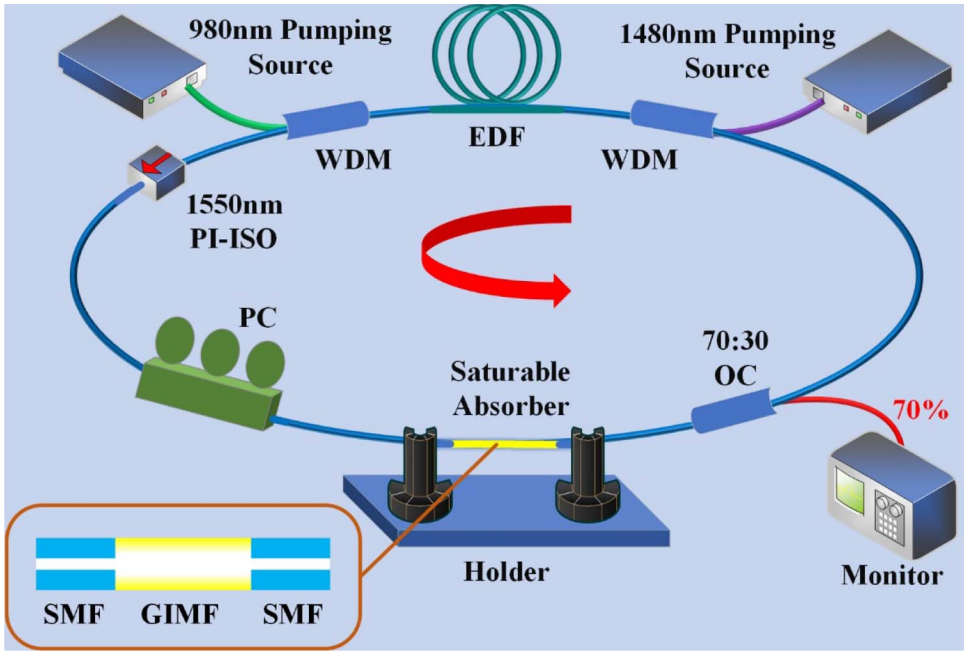

Fig. 4. Diagram of the large energy soliton oscillator. Red arrow represents the laser direction. WDM, wavelength division multiplexer; EDF, Er-doped fiber; PI-ISO, polarization independent isolator; PC, polarization controller; OC, optical coupler.

controller (PC), the GIMF-based SA, and a polarization-independent isolator (ISO). The EDF is simultaneously pumped by a 980 nm laser diode (LD) with an optical power of 600 mW and a 1480 nm LD with the power of 400 mW. The OC has an output ratio of 70%, which facilitates to extract the large energy pulse output. The PC is used to adjust the linear birefringence and optimize the mode-locking output. The ISO ensures the unidirectional operation of the cavity. All the components in the cavity are polarization independent to avoid the nonlinear polarization rotation effect. The net dispersion of the cavity is controlled by adding a section of SMF or dispersion compensated fiber (DCF) between the PC and the GIMF-based SA. The dispersion coefficients of SMF, DCF, and EDF used in the cavity are 18, −46.25, and −38 ps · nm^{-1} · km^{-1} in the wavelength region near 1.5 μm, respectively.

The output characteristics are monitored by use of an optical spectrum analyzer (Yokogawa, AQ6370D), an autocorrelator (APE, pulseCheck 150), an oscilloscope (Tektronix TDS5104B, 1 GHz) together with a 5 GHz photodetector (Thorlabs DET08CFC), a radio-frequency (RF) analyzer (SIGLENT SSA3032X), and a power meter (Thorlabs).

B. Large Energy Conventional Soliton Generation in the Anomalous Region

For the operation in the anomalous dispersion region with the total cavity length of ∼14 m, which yields an estimated net

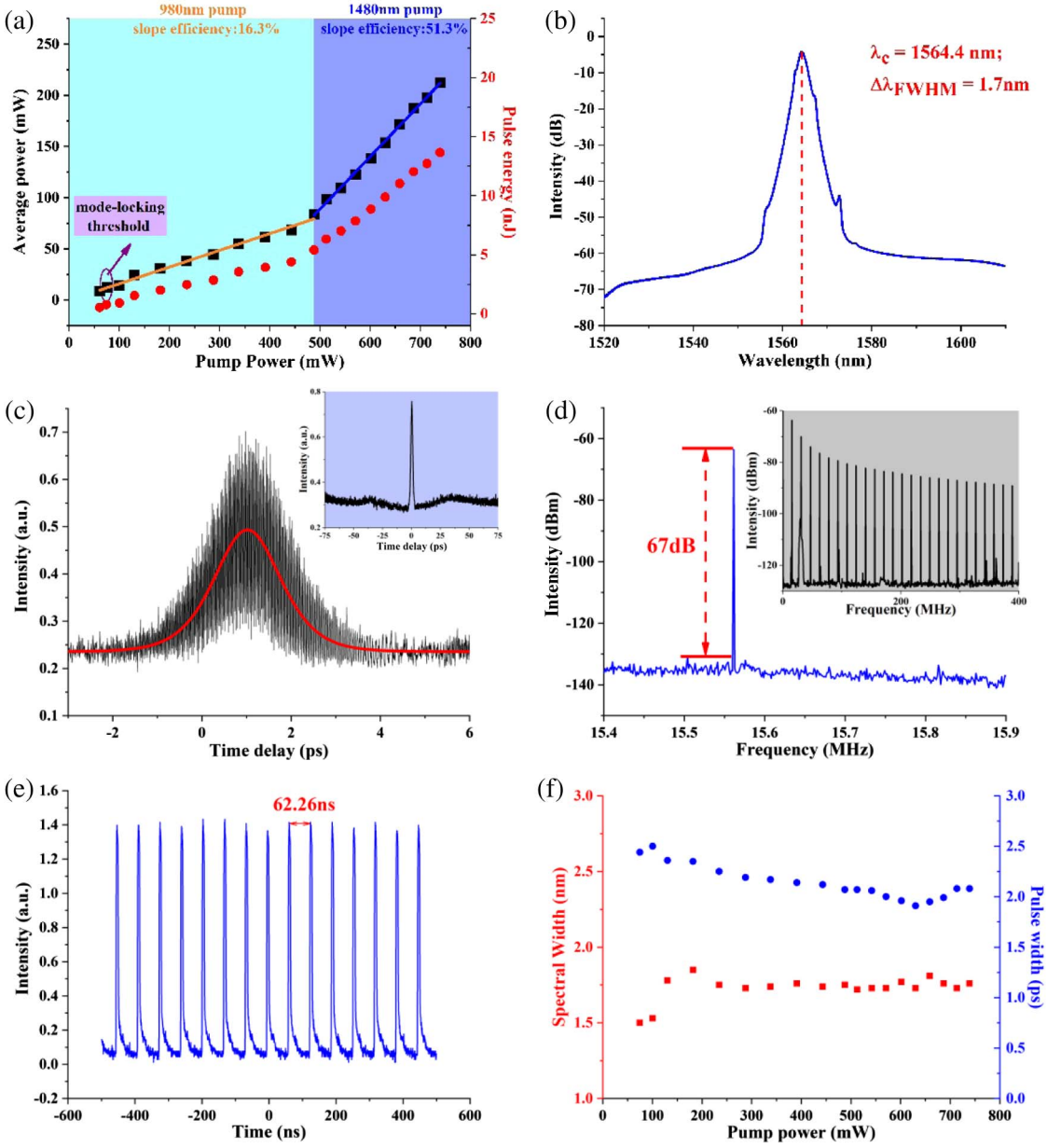

Fig. 5. Output characteristics of the mode-locking operation in the anomalous dispersion region. (a) Output power and pulse energy versus the pump power. (b) Optical spectrum at the maximum pump power. (c) Corresponding autocorrelation trace of the mode-locked pulse; inset is the autocorrelation trace with a large range of 150 ps. (d) Corresponding fundamental frequency of the RF spectrum; inset is the wideband RF spectrum within the 400 MHz span. (e) Digital oscilloscope image. (f) Spectral width and pulse width versus the pump power.

cavity dispersion of −0.233 ps^2, the self-started mode-locking operation was observed with the threshold pump power of 74.6 mW and an appropriate PC adjustment. As illustrated in Fig. 5(a), the output energy power demonstrates a linear increase with the efficiency slope of 16.3% at 980 nm and 51.3% at 1480 nm, respectively. The variation in the slope efficiency at different pump wavelengths is attributed to the higher gain coefficient of Er ions at 1480 nm. And no Q-switching, period-doubling, or higher-harmonic phenomenon was observed up to the maximum available pump power. The oscillator generated ultrafast pulses with the maximal average power of 212.4 mW at the fundamental repetition rate of 15.56 MHz, corresponding to the pulse energy of 13.65 nJ. To the best of our knowledge, this is the highest pulse energy for the single-mode Er-doped mode-locked fiber laser. It should be emphasized that the 212.4 mW output power is only contributed to the solitons emission in the 1560 nm regime, which is confirmed by the output pulse spectrum at the highest output power level with the central wavelength of 1564.4 nm and an FWHM value of the pulse width of 1.7 nm, as shown in Fig. 5(b). The pump power is almost entirely absorbed by the active fiber. Apart from this notable pulse energy extracted in the pure single-pulse regime directly obtained from a standard single-mode all-fiber Er^{3+}-doped oscillator mode locked by the GIMF-based SA, the noteworthy result is that these regimes are self-started directly from the CW regime, as marked in Fig. 5(a).

Although the net dispersion of the cavity is anomalous, no obvious Kelly sidebands are observed in the spectrum, as shown in Fig. 5(b). The spectral sidebands caused by periodic perturbations determine the shortest soliton in the cavity. The sideband amplitudes can be efficiently suppressed by controlling the fiber birefringence filtering effect [32] so as to increase the duration and quality of the pulses. Furthermore, the shape of the spectrum remains unchanged over the entire operation range. As shown in Fig. 5(c), the intensity autocorrelation trace of the output pulse has a width of 1.89 ps by assuming a sech^2 pulse profile. Thus, the time-bandwidth product is calculated to be 0.396, close to the Fourier limit if a sech^2 pulse is assumed. The peak power of the pulses is calculated to be 7.58 kW. A wide-span autocorrelation trace plotted confirms the single-pulse operation, as shown in the inset of Fig. 5(c).

Figure 5(d) shows the amplitude stability of the mode-locking operation in the frequency domain with a resolution of 10 Hz, from which we can see that the fundamental frequency is located at 15.56 MHz with a high-contrast level of exceeding 67 dB. This indicates that the solitons exhibit high stability. The single-pulse mode-locking operation can be further confirmed by the satellite-free long-range uniform envelope of the RF spectrum, as well as the output-pulse train in Fig. 5(e). Figure 5(f) records the evolution of the pulse width and the spectral bandwidth under different pump powers. The spectral width and the pulse width of the solitons do not change significantly with pump power, and no soliton instability has been observed in this process.

Usually, the maximum fundamental pulse energy E_s within tolerable limit is inversely proportional to the intensity of the nonlinear effect in the cavity, according to the soliton area theorem [32]

$$E_s = A_0\tau_p \propto \frac{\beta_2}{\gamma}, \tag{2}$$

where $\gamma = 1.08\ \mathrm{W^{-1}\cdot km^{-1}}$ at 1550 nm [10] is the fiber nonlinear coefficient, β_2 is the dispersion parameter, A_0 is the peak amplitude, and τ_p is the pulse duration. If the pump power is strongly enhanced beyond the threshold, the travelling solitons tend to break into multisoliton operation, which is responsible for the pulse energy limitation of common soliton fiber lasers.

In this experiment, the improvement of the pulse energy can be attributed to the following aspects. The Er-doped fiber is considered to have a smaller mode-field diameter (MFD) than that of the SMF, which is one of the main sources of the nonlinear effect generation inside the oscillator. Thus, shortening the length of EDF can lead to the considerable increase in the achievable pulse energy. In our experiment, the length of EDF with a relatively large MFD (∼8.8 μm) and a large absorption coefficient is chosen to be ∼70 cm, which is the shortest possible while ensuring sufficient gain. The use of the output coupler with higher coupling ratio (70%) in the laser cavity could also be an important factor to increase the soliton pulse energy. Furthermore, our SA exhibits low scattering loss, high optical damage threshold, enhanced modulation depth, and small saturation intensity, which are important factors in high power operation of the laser. Hence, by these means, the nonlinearity in the cavity can be effectively reduced, and the high pulse energy is realized. It is believed that the soliton pulse energy could be further improved by optimizing the laser cavity design.

Meanwhile, in order to further investigate the stability of the generated mode-locking solitons, a long-term stability examination of the Er-doped soliton fiber laser under the laboratory condition has been conducted. Figure 6 shows the measurement results over 15 h. It can be seen from the figure that the relative output power fluctuation is small and estimated to be less than 5%. Such a value is acceptable for a high-energy soliton fiber laser.

For the operation in the normal dispersion with the total cavity length of ∼17 m, including a section of 10 m DCF (the corresponding total dispersion is 0.336 ps^2), a dissipative soliton with the maximum average power of 72.6 mW at the repetition rate of 11.63 MHz is obtained at the pump power of 495 mW, which corresponds with the maximum pulse energy of 6.25 nJ, as shown in Fig. 7(a). The laser efficiency is 10.6%

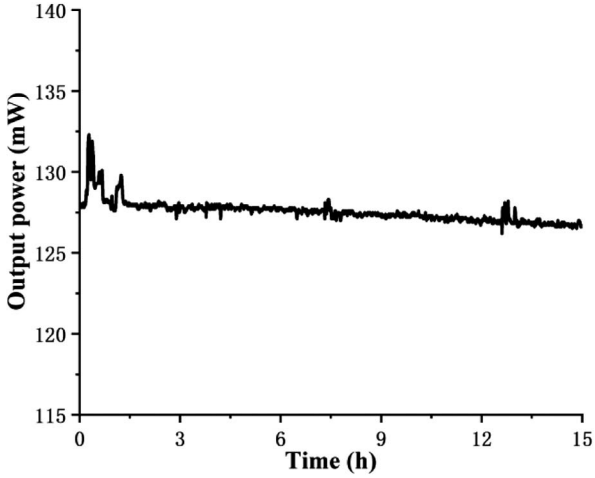

Fig. 6. Measured laser output power over 15 h.

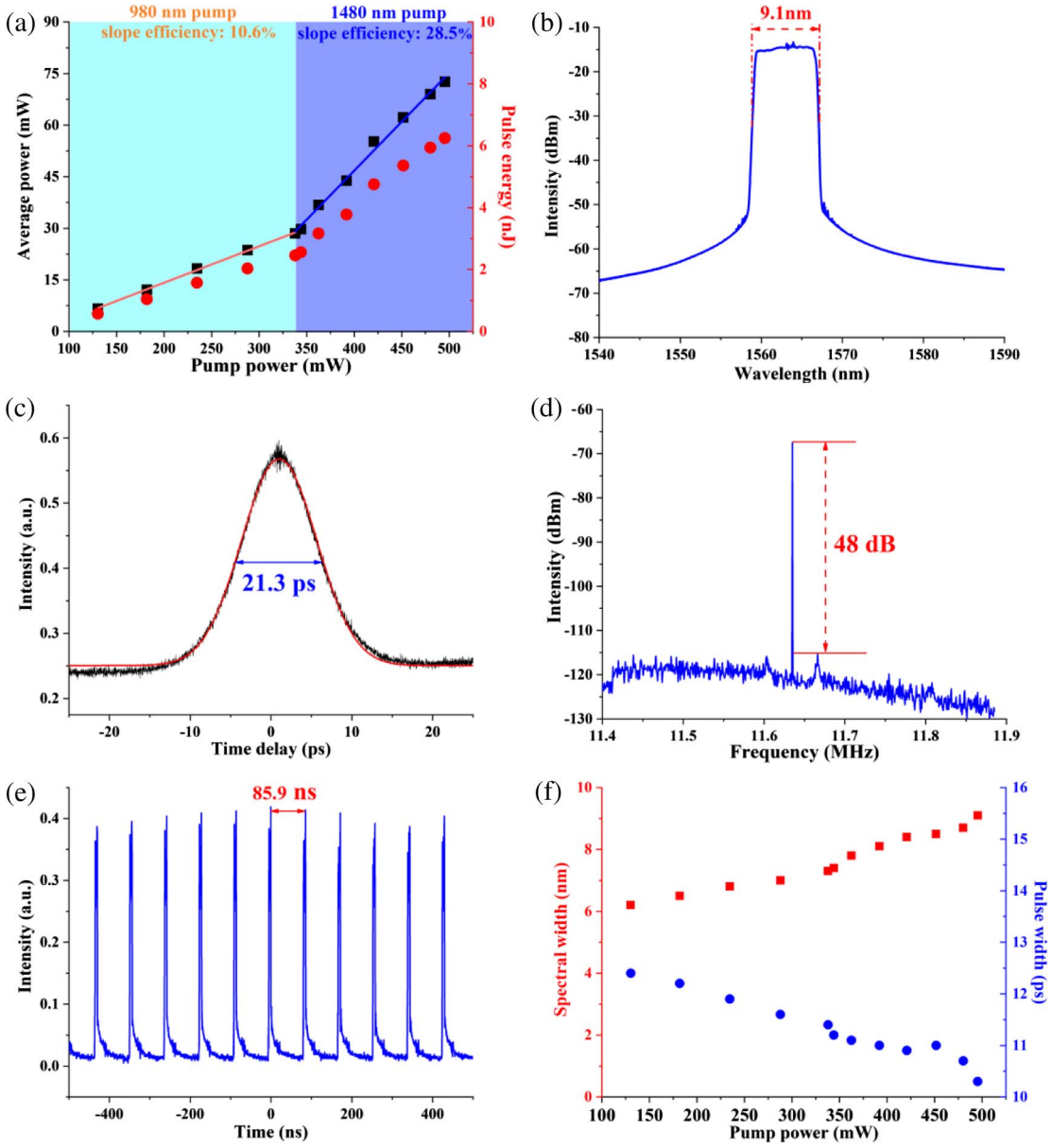

Fig. 7. Output characteristics of the mode-locking operation in the anomalous dispersion region. (a) Output power and pulse energy versus the pump power. (b) Optical spectrum at the maximum pump power. (c) Corresponding autocorrelation trace of mode-locked pulse. (d) Corresponding fundamental frequency of the RF spectrum. (e) Digital oscilloscope image. (f) Spectral width and pulse width versus the pump power.

at 980 nm and 28.5% at 1480 nm, respectively. It can be seen from the figure that the slope efficiency in the normal regime is decreased obviously compared with that in the anomalous dispersion region. In our experiment, the increase of the cavity length decreases the repetition frequency of the solitons, which leads to a lower gain efficiency. The mode field mismatch between SMF and DCF during fusion splicing introduces additional loss in the cavity. The reasons mentioned above explain the decrease of the slope efficiency in the normal regime. Furthermore, the increase of DCF length with a relatively small mode area leads to the excessively accumulated nonlinear effect and reduced mode-locking stability. Pulse splitting occurs at the relatively high level of pump power; thus, the mode-locked oscillator in the anomalous dispersion regime can support a higher-energy soliton pulse than that in the positive regime. Figure 7(b) shows the output spectrum centered at 1563 nm with an edge-to-edge width of 9.1 nm. The spectrum exhibits steep side edges that are typical characteristics of the dissipative solitons in large positive dispersion lasers. The output pulses have a large positive chirp and, by assuming a Gaussian pulse profile, the pulse duration of ~21.3 ps is obtained, as shown in Fig. 7(c). The RF spectrum and the output pulse train are displayed in Figs. 7(d) and 7(e), respectively. The narrow linewidth of the RF peaks centered at 11.63 MHz as well as the constant height of 48 dB over the flat noise-underground confirms that no Q-switching, period-doubling, or higher-harmonic mode-locking exists. Compared with the operation in the anomalous regime, the stability of the solitons is reduced,

due to the increase of the laser cavity length. During the process of the pump power increasing from 130 to 500 mW, the edge-to-edge spectral width of the output spectrum is broadened from 9.1 to 15 nm due to the SPM effect; further, the corresponding pulse width is compressed from 12.4 to 10.7 ps.

4. CONCLUSION

In conclusion, we have constructed a type of GIMF-based SA with an all-fiber structure for pulse energy enhancement. Such an SA demonstrates superior properties of large damage threshold, large modulation depth of 29.6%, small saturation fluence of $\sim 7.19 \times 10^{-3}$ μJ/cm^2, and small nonsaturable loss of 26.1%, which are excellent mode-locking abilities for stable large energy soliton generation. Once employed in the EDF oscillator in the anomalous and normal regimes, the large energy CSs and DSs can be generated, respectively. The energy of 1.89 ps CSs is up to 13.65 nJ and that of 21.3 ps DSs is up to 6.25 nJ. The experimentally obtained results show that the GIMF-based SA is attractive for high-energy soliton generation. Moreover, further energy scaling is possible if a double-clad Er-doped fiber with a large core is employed.

Funding. National Natural Science Foundation of China (61805225).

REFERENCES

1. A. Schneider, M. Stillhart, and P. Günter, "High efficiency generation and detection of terahertz pulses using laser pulses at telecommunication wavelengths," Opt. Express **14**, 5376–5384 (2006).
2. J. Kim and Y. Song, "Ultralow-noise mode-locked fiber lasers and frequency combs: principles, status, and applications," Adv. Opt. Photon. **8**, 465–540 (2016).
3. G. Krauss, S. Lohss, T. Hanke, A. Sell, S. Eggert, R. Huber, and A. Leitenstorfer, "Synthesis of a single cycle of light with compact erbium-doped fibre technology," Nat. Photonics **4**, 33–36 (2010).
4. F. Ilday, J. Buckley, W. Clark, and F. Wise, "Self-similar evolution of parabolic pulses in a laser," Phys. Rev. Lett. **92**, 213902 (2004).
5. J. W. Nicholson, A. D. Yablon, P. S. Westbrook, K. S. Feder, and M. F. Yan, "High power, single mode, all-fiber source of femtosecond pulses at 1550 nm and its use in supercontinuum generation," Opt. Express **12**, 3025–3034 (2004).
6. L. Duan, X. Liu, D. Mao, L. Wang, and G. Wang, "Experimental observation of dissipative soliton resonance in an anomalous-dispersion fiber laser," Opt. Express **20**, 265–270 (2012).
7. T. Du, Z. Luo, R. Yang, Y. Huang, Q. Ruan, Z. Cai, and H. Xu, "1.2-W average-power, 700-W peak-power, 100-ps dissipative soliton resonance in a compact Er:Yb co-doped double-clad fiber laser," Opt. Lett. **42**, 462–465 (2017).
8. M. Olivier, V. Boulanger, F. Guilbert-Savary, P. Sidorenko, F. W. Wise, and M. Piché, "Femtosecond fiber Mamyshev oscillator at 1550 nm," Opt. Lett. **44**, 851–854 (2019).
9. W. Liu, R. Liao, J. Zhao, J. Cui, Y. Song, C. Wang, and M. Hu, "Femtosecond Mamyshev oscillator with 10-MW-level peak power," Optica **6**, 194–197 (2019).
10. H. H. Liu and K. K. Chow, "Enhanced stability of dispersion-managed mode-locked fiber lasers with near-zero net cavity dispersion by high-contrast saturable absorbers," Opt. Lett. **39**, 150–153 (2014).
11. C. Lecaplain, M. Baumgartl, T. Schreiber, and A. Hideur, "On the mode-locking mechanism of a dissipative- soliton fiber oscillator," Opt. Express **19**, 26742–26751 (2011).
12. J. Wang, Z. Jiang, H. Chen, J. Li, J. Yin, J. Wang, T. He, P. Yan, and S. Ruan, "High energy soliton pulse generation by a magnetron-sputtering-deposition-grown $MoTe_2$ saturable absorber," Photon. Res. **6**, 535–541 (2018).
13. H. Zhang, D. Y. Tang, L. M. Zhao, Q. L. Bao, and K. P. Loh, "Large energy mode locking of an erbium-doped fiber laser with atomic layer graphene," Opt. Express **17**, 17630–17635 (2009).
14. K. Kieu and M. Mansuripur, "Femtosecond laser pulse generation with a fiber taper embedded in carbon nanotube/polymer composite," Opt. Lett. **32**, 2242–2244 (2007).
15. A. Betlej, S. Suntsov, K. G. Makris, L. Jankovic, D. N. Christodoulides, G. I. Stegeman, J. Fini, R. T. Bise, and D. J. DiGiovanni, "All-optical switching and multifrequency generation in a dual-core photonic crystal fiber," Opt. Lett. **31**, 1480–1482 (2006).
16. T. F. S. Büttner, D. D. Hudson, E. C. Mägi, A. Casas Bedoya, T. Taunay, and B. J. Eggleton, "Multicore, tapered optical fiber for nonlinear pulse reshaping and saturable absorption," Opt. Lett. **37**, 2469–2471 (2012).
17. H. C. Nguyen, D.-I. Yeom, E. C. Mägi, B. T. Kuhlmey, C. M. de Sterke, and B. J. Eggleton, "Nonlinear switching using long-period gratings in As_2Se_3 chalcogenide fiber," J. Opt. Soc. Am. B **25**, 1393–1401 (2008).
18. T. Chen, Q. Zhang, Y. Zhang, X. Li, H. Zhang, and W. Xia, "All-fiber passively mode-locked laser using nonlinear multimode interference of step-index multimode fiber," Photon. Res. **6**, 1033–1039 (2018).
19. E. Nazemosadat and A. Mafi, "Nonlinear multimodal interference and saturable absorption using a short graded-index multimode optical fiber," J. Opt. Soc. Am. B **30**, 1357–1367 (2013).
20. L. G. Wright, W. H. Renninger, D. N. Christodoulides, and F. W. Wise, "Spatiotemporal dynamics of multimode optical solitons," Opt. Express **23**, 3492–3506 (2015).
21. G. Lopez-Galmiche, Z. Sanjabi Eznaveh, M. A. Eftekhar, J. Antonio Lopez, L. G. Wright, F. Wise, D. Christodoulides, and R. A. Correa, "Visible supercontinuum generation in a graded index multimode fiber pumped at 1064 nm," Opt. Lett. **41**, 2553–2556 (2016).
22. H. Pourbeyram and A. Mafi, "Photon pair generation with tailored frequency correlations in graded-index multimode fibers," Opt. Lett. **43**, 2018–2021 (2018).
23. U. Teğin and B. Ortaç, "All-fiber all-normal-dispersion femtosecond laser with a nonlinear multimodal interference-based saturable absorber," Opt. Lett. **43**, 1611–1614 (2018).
24. Z. Lv, Z. Yang, D. D. Song, F. Li, X. Yang, Y. Yang, Y. Wang, Q. Li, and W. Zhao, "Nonlinear multimodal interference for ytterbium-doped all-fiber mode-locking noise-like pulse generation," Appl. Phys. Express **12**, 022004 (2019).
25. G. Chen, W. Li, G. Wang, W. Zhang, C. Zeng, and W. Zhao, "Generation of coexisting high-energy pulses in a mode-locked all-fiber laser with a nonlinear multimodal interference technique," Photon. Res. **7**, 187–192 (2019).
26. Z. Wang, D. N. Wang, F. Yang, L. Li, C.-L. Zhao, B. Xu, S. Jin, S.-Y. Cao, and Z.-J. Fang, "Stretched graded-index multimode optical fiber as a saturable absorber for erbium-doped fiber laser mode locking," Opt. Lett. **43**, 2078–2081 (2018).
27. H. Li, F. Hu, Y. Tian, P. Wang, J. Zhang, and S. Xu, "Continuously wavelength-tunable mode-locked Tm fiber laser using stretched SMF-GIMF-SMF structure as both saturable absorber and filter," Opt. Express **27**, 14437–14446 (2019).
28. H. Li, F. Hu, C. Li, Y. Tian, C. Huang, J. Zhang, and S. Xu, "Generation of switchable multiwavelength solitons with wide wavelength spacing at 2 μm," Opt. Lett. **44**, 2442–2445 (2019).
29. A. Mafi, P. Hofmann, C. J. Salvin, and A. Schülzgen, "Low-loss coupling between two single-mode optical fibers with different mode-field diameters using a graded-index multimode optical fiber," Opt. Lett. **36**, 3596–3598 (2011).
30. J. W. Jeon, J. S. Lee, and J. H. Lee, "Numerical study on the minimum modulation depth of a saturable absorber for stable fiber laser mode locking," J. Opt. Soc. Am. B **32**, 31–37 (2015).
31. S. Minardi, G. Cheng, C. D'Amico, and R. Stoian, "Low-power-threshold photonic saturable absorber in nonlinear chalcogenide glass," Opt. Lett. **40**, 257–259 (2015).
32. L. E. Nelson, D. J. Jones, K. Tamura, H. A. Haus, and E. P. Ippen, "Ultrashort-pulse fiber ring lasers," Appl. Phys. B **65**, 277–294 (1997).